

Medical applications of surface-enhanced Raman scattering

Cite this: *Phys. Chem. Chem. Phys.*, 2013, **15**, 5329

Wei Xie and Sebastian Schlücker*

Received 31st October 2012,
Accepted 26th February 2013

DOI: 10.1039/c3cp43858a

www.rsc.org/pccp

This perspective article provides an overview of selected medical applications of surface-enhanced Raman scattering (SERS), highlighting recent developments and trends. The use of SERS for detection, analysis and imaging has attracted great interest in the past decade owing to its high sensitivity and molecular fingerprint specificity. SERS can deliver chemical and structural information from analytes rapidly and nondestructively in a label-free manner. Alternatively, SERS labels or nanotags, when conjugated to target-specific ligands, can be employed for the selective detection and localization of the corresponding target molecule. Biomedical applications based on both approaches are highlighted.

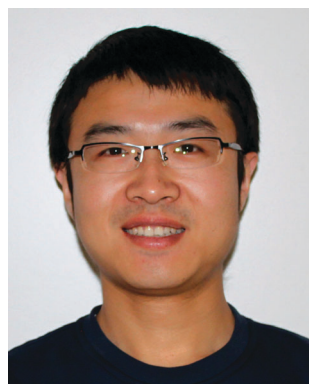
1. Introduction

Surface-enhanced Raman scattering (SERS) is a sensitive and selective spectroscopic technique for molecular detection and identification. SERS requires the excitation of a localized surface plasmon resonance (LSPR) by an incident electromagnetic wave.^{1–3} The magnitude of the Raman scattering intensity is significantly enhanced when the molecules are placed in the local LSPR fields. SERS inherits all the advantages of normal Raman spectroscopy such as abundant spectral information and low water interference; on the other hand, it overcomes the inherent

problem of low sensitivity in electronically non-resonant Raman spectroscopy, which renders SERS to be a highly sensitive and surface-selective “fingerprint” method.⁴ In the past decade, it has been used extensively in many important research areas, in particular physical^{5–7} and analytical^{8–13} chemistry.

SERS has long been regarded as a promising analytical technique for medical samples, which usually have a complex biochemical composition and predominantly contain water.¹⁴ On the other hand, nanostructured materials are excellent candidates as probes because they can produce a high response to very small targets under practical conditions.¹⁵ Gold (Au) and silver (Ag) nanoparticles (NPs) can not only be used as plasmonically active substrates for label-free SERS detection, but also be functionalized with Raman reporter molecules (SERS labels/nanotags)

Department of Chemistry, University of Duisburg-Essen, Universitätsstr. 5, 45141 Essen, Germany. E-mail: sebastian.schluecker@uni-due.de



Wei Xie

Wei Xie studied chemistry and received his doctoral degree in analytical chemistry from Wuhan University, China, in 2009. He then joined the Schlücker labs at the University of Osnabrück for postdoctoral work as an Alexander von Humboldt fellow. His research interests include the rational design and synthesis of multifunctional plasmonic nanoparticles for SERS applications, in particular catalysis.



Sebastian Schlücker

Sebastian Schlücker received his doctoral degree in physical chemistry from the University of Würzburg, Germany, in 2002, and postdoctoral training at the US NIH. In 2008 he joined the Physics Department at the University of Osnabrück, since 2012 he has been with the Faculty of Chemistry at the University of Duisburg-Essen. His research interests include the rational design and synthesis of multifunctional plasmonic nanoparticles for SERS applications, in particular for tissue-based cancer diagnostics.

and target-specific ligands such as antibodies. The corresponding NP–ligand conjugate can thereby recognize the corresponding target molecule for the selective detection of target molecules in complex biological systems. A strongly enhanced Raman signal from the target in very close vicinity of the metal substrate surface (label-free SERS), or from Raman reporter molecules on the metal surface (SERS labels), can be used for efficient detection and discrimination of the target molecules from the background.

In this perspective paper, selected medical applications of SERS from the past few years are highlighted. Both aspects – the label-free SERS detection of biomedical samples (Section 2) as well as the use of SERS labels (Section 3) in medical applications – will be covered.

2. Label-free SERS detection in medical applications

SERS can deliver abundant molecular structural information directly from aqueous biomedical samples, which may be difficult or even not be possible by other spectroscopic techniques. This unique advantage in combination with its molecular specificity enables SERS to be used for label-free detection in medical studies.

2.1 Quantitative detection of *Legionella pneumophila* and *Salmonella typhimurium*

A quantitative and straightforward detection method in aqueous solution is important for the identification of pathogenic microorganisms. Ideally, such a method enables a fast and inexpensive diagnosis. Haisch and co-workers reported the label-free SERS detection of *Legionella pneumophila* and *Salmonella typhimurium* cells.¹⁶ By using a SERS-based immunoassay, the determination of bacterial contamination in water does not require enrichment or dehydration steps prior to analysis and labeling can also be avoided. The total assay time is only 65 minutes. Before the SERS measurement, the bacterial suspension was incubated on a glass chip containing the respective antibodies, anti-*Legionella* antibody or anti-*Salmonella* antibody. After the cells were captured and immobilized on the glass chip, the chip was placed in a polycarbonate tray which was filled with a Ag colloid. The corresponding SERS spectra of the bacteria showed only weak signals in the fingerprint region. The addition of sodium azide during the incubation with the Ag colloid induced specific agglomeration of the Ag NPs at the site of the bacterial cell wall, resulting in a significant SERS signal enhancement. Reliable identification of the bacteria was possible by means of their whole-organism fingerprint spectra, where *L. pneumophila* showed strong peaks of amide I, II, and III and *S. typhimurium* exhibited strong peaks only of amide II and III. Reproducible spectra were measured from several cells of the same colony. For quantification, SERS mapping on the chip was carried out according to their amide III band, for *S. typhimurium* at 1290 cm⁻¹ and *L. pneumophila* at 1310 cm⁻¹. If the signal intensity was stronger than 6 times that of the standard deviation of background spectra, it was defined as a positive detection. The number of positive detections within a

600 μm × 600 μm area on the chip surface was used to quantify the concentration of bacterial cells. Concentrations between 10⁶ and 10⁹ cells per mL were examined for *S. typhimurium* and between 10⁸ and 10⁹ cells per mL for *L. pneumophila*.

2.2 SERS detection of folic acid using graphene oxide–Ag NP hybrids

Folic acid, also known as vitamin B, is related to many diseases including heart attacks, congenital malformation and mental devolution.^{17–19} Graphene oxide–Ag NP hybrid structures were synthesized and used to detect folic acid in aqueous solution and in serum according to the intrinsic Raman/SERS spectrum of folic acid.²⁰ Hybrid SERS substrates were prepared by self-assembly of Ag NPs on graphene oxide. The modification of graphene oxide with positively charged poly(diallyldimethyl ammonium chloride) (PDDA) was employed for the electrostatic self-assembly of the negatively charged Ag NPs onto PDDA-coated graphene. The assembly of Ag NPs reduced the interparticle distance and therefore increased the SERS activity. More importantly, the positive surface charge of the final hybrid substrates is capable of enriching the folic acid molecules *via* electrostatic attraction, which provided a further enhancement of the SERS signal. The limit of detection for folic acid in aqueous solution was 9 nM, and the calibration curve showed a good linear relation in the concentration range from 9 to 180 nM. A known amount of folic acid in serum was tested with the same method and the sensitivity and the linear response range were comparable to that in aqueous solution. The spectral influence from the proteins in the serum was almost negligible.

2.3 Intracellular monitoring of thiopurine anticancer drug release

Purine analogues can be used as antileukemic and antineoplastic drugs for the treatment of cancers. Most anticancer drug release studies using fluorescence techniques require additional fluorescent dyes. Ock *et al.* recently investigated thiopurine anticancer drug release *in vitro* and *in vivo* using SERS and live cell imaging techniques without use of any additional tagging molecules.²¹ 6-Mercaptopurine (6MP) and 6-thioguanine (6TG) adsorbed on the surface of Au NPs were replaced by glutathione monoester (GSH-OEt) as an intracellular external stimulus (Fig. 1A). The release of a portion of 6MP or 6TG molecules adsorbed on the Au NPs was observed by monitoring the decrease in the corresponding SERS intensity. A tripeptide with a methyl group instead of a thiol group was used as an inactive GSH derivative in a negative control experiment. Fig. 1B shows the change in SERS intensity in aqueous suspension as a function of GSH concentration. The strongest Raman band, which can be assigned to the C–N stretching of the purine ring, was used to monitor the decrease in SERS intensity. Monitoring the release of thiopurine drugs using intracellular endogenous GSH was performed by adding GSH-OEt into the cell culture medium (Fig. 1C). The decrease in the band intensities depends on the elapsed time after the addition of GSH-OEt. *In vivo* SERS studies on the drug release in living mice were also attempted

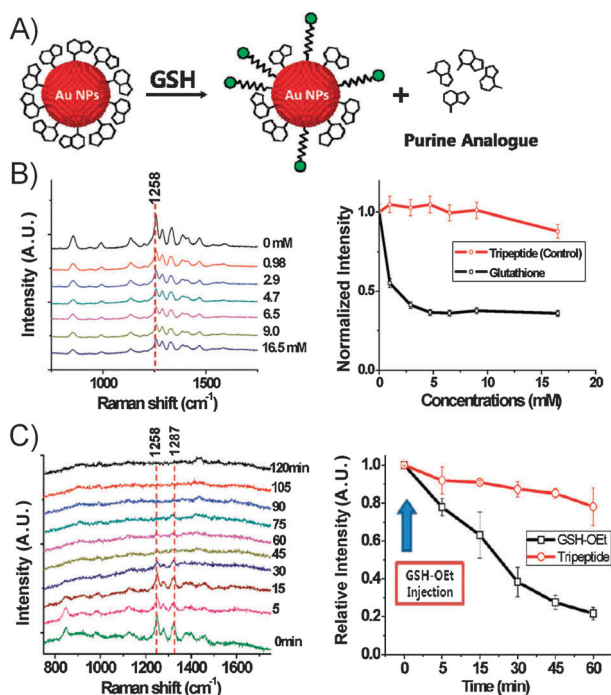


Fig. 1 (A) Release of thiopurine adsorbed on Au NPs via GSH. (B) GSH concentration-dependent SERS intensity of 6MP adsorbed on Au NPs suspended in water. (C) Time-lapse SERS experiment in A549 cells after treatment of GSH-OEt, indicating the *in situ* desorption of 6MP from the Au NP surface. From ref. 21.

by subcutaneous injection of 6TG modified Au NPs. The SERS signal was obtained from the subcutaneous site upon 785 nm excitation. The band intensity of 6TG appeared to decrease when GSH-OEt was injected, whereas the control tripeptide did not show much influence.²¹

2.4 Tubing sensor for SERS monitoring of intravenous drugs and metabolites

Flexible plastic tubings are widely used in medical treatments, including intravenous delivery, urinary catheterization and dialysis. Continuous monitoring of chemical components in the liquid flowing through the tubing has been realized by incorporation of label-free SERS sensors into the internal surfaces of the plastic tubing.²² First, a SERS-active nanodome surface was fabricated by replica molding of a polymer on a silicon template and electron-beam evaporation of Ag on the replicated polymer surface. Then this SERS sensor was placed in a flow cell, which can be connected to plastic tubes for medical treatment (Fig. 2). Promethazine and a common urinary metabolite (urea) were detected as model analytes to demonstrate the potential of the method for continuous monitoring of a delivered drug or kidney function of a patient. SERS spectra were obtained from the sensor through the glass window. The intensities of Raman bands at 1000 and 1030 cm⁻¹, which are assigned to the ring-breathing mode of promethazine and the symmetrical C–N stretching mode of urea, respectively, were used to determine the concentration of the corresponding analytes. Both linear fits – plotting the

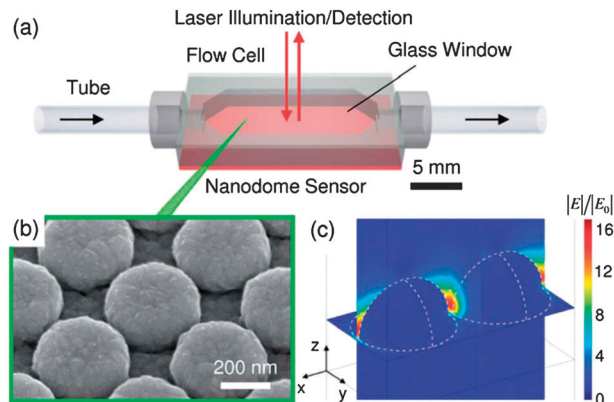


Fig. 2 (a) Schematic of the sensor tubing, in which a nanodome sensor structure is incorporated as the bottom surface of the flow cell. (b) SEM image of the nanodome surface. (c) 3D FEM simulation of the electric field distribution displaying regions of enhanced field between adjacent nanodomains. From ref. 22.

Raman intensity as a function of the concentration of the corresponding compounds – yielded an R^2 value of 0.999, which demonstrates that this label-free method can be used for the quantitative detection of drugs and metabolites.

2.5 Glucose sensing by SERS

Patients with diabetes mellitus require frequent monitoring of their glucose levels. Most patients use a “finger-stick” apparatus for withdrawing small samples of blood in a painful and inconvenient way. Therefore, many research groups are trying to develop minimally invasive and biologically compatible methods for quantitative glucose detection. Silver film over nanospheres (AgFON) as the SERS substrate in combination with partial least squares (PLS) as a chemometric method was successfully employed for quantitative glucose sensing. A key element is the use of a partition layer on the surface of the AgFON substrate for generating a glucose concentration gradient.²³ A dozen different partition layers were studied, but only straight alkanethiols were found to be effective; in this study, 1-decanethiol (1-DT) was employed. It is important to note that without this partition layer, SERS of glucose could not be observed since the necessary preconcentration – bringing glucose molecules in close vicinity to the plasmonic AgFON surface – is missing in this case.

More recently, *in vivo* transcutaneous glucose sensing on rat models was developed.^{24,25} AgFON surfaces were functionalized with a mixed self-assembled monolayer (SAM) of 1-DT and 6-mercapto-1-hexanol (MH) (Fig. 3), and implanted subcutaneously in living rats. The 1-DT/MH SAM was designed to have dual hydrophobic–hydrophilic functionality, which performed better as a partitioning layer than the layer used before because hydroxyl-terminated chains formed hydrophilic pockets and partition glucose closer to the SERS active surface.²⁶ The SAM also excluded nontarget molecules like proteins that could give rise to spectral congestion. For the subcutaneous implantation, an incision was made in the skin of a rat and a pocket was blunt dissected into the subcutaneous space. A single 6-DT/MH@AgFON was placed in the pocket. All incisions were closed with surgical clips.

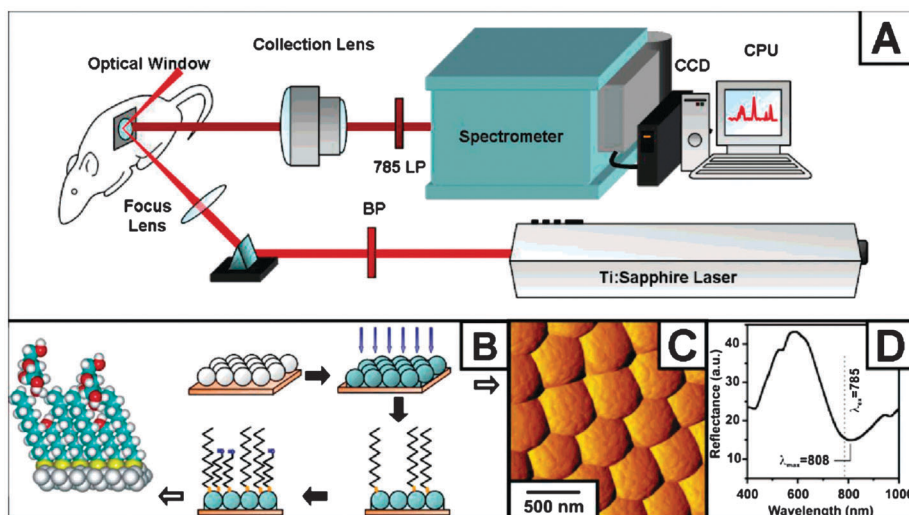


Fig. 3 (A) Schematic of instrumental apparatus for glucose sensing *in vivo*. (B) AgFONs were prepared by depositing metal through a mask of self-assembled nanospheres. The AgFON was then functionalized by successive immersions in ethanolic solutions of 1-DT and MH. Glucose is able to partition into and out of the DT/MH layer. (C) The resulting structure is shown in the atomic force micrograph. (D) After functionalization, a reflectance spectrum was collected to determine the position of the LSPR peak. From ref. 24.

The glucose concentration in the rat was increased through intermittent intravenous infusion and decreased by intravenous insulin injection over the course of the experiment. The glucose concentration was monitored in the interstitial fluid of six separate rats. The sensor was able to perform accurately over lower glucose concentrations over 17 days after subcutaneous implantation.²⁵

2.6 Targeted label-free SERS detection of living cells

Label-free SERS detection provides molecular structural information directly from samples, which can be used for *in situ* studies on the interaction between anticancer drugs and cells at the subcellular level. SERS was first used in living cells in 2002 for intracellular detection of native chemical constituents; the Au NPs were incorporated in the intestinal epithelial cells by passive uptake.²⁷ Cells are complex biological specimens with organelles and many different biochemical components. Correspondingly, the analysis of the corresponding SERS spectra is challenging and time consuming. This complexity is reduced when the NPs are localized only in selected cellular organelles for selectively probing their chemical composition. Nuclear-targeted SERS detection of a single living cell has been performed by using peptide-functionalized Au NPs.²⁸ The cell nucleus is a desirable target since the genetic information and transcription machinery resides there. SV-40 large T nuclear localization signal (NLS) peptide derived from the virus facilitates the transport of Au NPs into the cell nucleus. The conjugation of the NLS peptide and the Au NPs is very important in the preparation of the label-free SERS nanoprobe. In label-free SERS detection, adsorption or compact adjacency of the analyte and the metal surface is required. If the metal surface was fully covered, or if the functionalization imposed too much influence on the SERS detection, the Au NPs could not be used to detect the Raman signal from cellular components.

The NLS peptide was conjugated to 20 nm Au NPs modified with a small amount of 11-mercaptopundecanoic acid (11-MUA), which has a minor impact on SERS detection, to avoid full surface coverage and spectral influence. The nanoprobe enters the cell nucleus after the incubation with HeLa cells and delivers the spatially localized chemical information of the nucleus. The nanoprobe was also used to detect molecules intruded to demonstrate the ability to study drug–nucleus interactions.²⁸ After incubation with the nanoprobe, the living cells were stained with DAPI, a DNA intercalator as the model for the drug–nucleus interaction study. The SERS signal from the cell nucleus indicated that DAPI molecules might insert *via* minor-groove binding at adenine–thymine sites of the DNA.

2.7 SERS label-free detection of single-base mismatches in DNA

Analysis of DNA sequences and characterization of single-nucleotide polymorphisms (SNPs) are both important for medical diagnosis because changes in the DNA sequence may cause inherited disorders. MALDI-TOF mass spectrometry, which is extensively used in SNP genotyping methods, is expensive and offsets the significant advantage of being able to avoid labeling steps in the analysis. SERS is an alternative method which combines high sensitivity with low cost. Label-free SERS detection of DNA normally requires thiolated sequences, which give the DNA a more tilted orientation that prevents all the bases from interaction with the metal surface. SERS spectra of thiolated DNA are dominated by adenine signals.²⁹ Label-free SERS detection of unthiolated DNA sequences has been achieved by MgSO₄ induced aggregation of Ag NPs.³⁰ The obtained SERS spectra showed features associated with all the constituent bases. It is important to mention that if the colloid is aggregated by a high concentration of NaCl, no DNA Raman signals can be observed because the DNA molecules do not

attach to the metal surface in the presence of high (0.1 M) NaCl concentrations. Each polymorphism gives a different pattern of spectral changes. DNA sequences with one base difference were tested to demonstrate the ability to detect A to G and C to A polymorphisms, respectively. When a single A is replaced by G in a 25-mer DNA sequence, the SERS difference spectrum showed a good agreement with the model spectrum created by subtracting the spectrum of the poly-A sequence from that of deoxyguanosine monophosphate (dGMP). Also, when a single C is replaced by A in a 23-mer sequence, a good agreement between the difference spectrum and the model, obtained by subtracting the spectrum of poly C from that of poly A, is observed. The study indicates that single-base mismatches in short DNA strands can be identified by SERS.

2.8 Label-free SERS detection schemes: a critical perspective

Every analytical technique has its own characteristic advantages and disadvantages. First of all, SERS is a surface-selective technique, which has an important analytical consequence: the analyte must be placed in very close vicinity of the metal surface for efficient detection. Therefore, label-free SERS detection schemes are usually limited to molecules with surface-seeking groups. For example, the release of the thiopurine anticancer drug (Section 2.3) can be efficiently monitored by SERS only because of its surface-seeking thiol group. However, the same method cannot be simply applied to molecules without any surface-seeking group. Strategies for capturing the analyte on the surface of the SERS substrate are promising methods for circumnavigating this issue. Examples from the SERS literature include 4-nitrophenol captured by a thermally responsive porous poly-(*N*-isopropylacrylamide) shell on Au NPs,³¹ and polyaromatic hydrocarbons captured by supramolecular host-guest interactions.³²

The second inherent shortcoming of label-free SERS detection is the small Raman cross section of certain analytes. Although all molecules in principle can produce SERS since all molecules have Raman-active vibrations (even H₂ does), not all molecules are good SERS samples due to their Raman scattering cross sections.³³ In practice, many molecules in medical studies do not have sufficiently high Raman cross sections for label-free SERS detection. In other words, even if they would be close enough to the metal surface (irrespective of an available surface-seeking group or not), they could not be detected at very low concentrations (and moderate field enhancements). The enrichment of analytes close to the metal surface is a promising method to detect sample molecules with small cross sections. For example, glucose molecules enriched by a SAM on a AgFON surface (Section 2.5) can be detected by SERS.²³ Such intelligent strategies require physical and chemical knowledge of interfaces and the corresponding intermolecular forces.

A third important aspect is the balance between sensitivity/signal strength and reproducibility. Unfortunately, present plasmonic nanostructures do not simultaneously provide extreme sensitivity (field enhancements) and extreme reproducibility (same field enhancement at every location). Hot spots exhibit

extreme field enhancements, but they are highly localized (see Section 2.4, Fig. 2c) and in many cases difficult to control. The synthesis/fabrication of novel plasmonic nanostructures with high SERS activity and structural reproducibility at the same time will therefore be an integral part of future label-free SERS work.

3. SERS labels in medical diagnostic studies

The examples in Section 2 demonstrate that SERS can be employed for label-free detection of certain biomolecular systems, microorganisms, cancer markers, and certain other medically relevant analytes, usually molecules with surface-seeking groups. The complex biochemical composition of biological specimen makes the interpretation of SERS spectra challenging and the identification of a particular biomolecular system of interest is far from being trivial. These constraints have led to the development of SERS labels or nanotags for medical and bioanalytical applications, very similar to the technique of labeling with fluorescent dyes or quantum dots.

A SERS label or nanotag consists of three central components: (1) Raman reporter molecules to provide characteristic Raman bands as readout signal; (2) a plasmonically active metal nanostructure (colloidal or solid SERS substrate) with strong electromagnetic fields to enhance the Raman signal from the reporter molecules upon resonant laser excitation; (3) a ligand for recognizing the corresponding target molecule. These three components are usually integrated into a single nanoparticle entity. Typically, a shell is also used for chemical and mechanical stabilization of the actual SERS label.³⁴

3.1 Detection of DNA by SERS labels

3.1.1 SERS-melting for discriminating mutations in DNA sequences. Discrimination of genomic mutations in DNA is important for DNA-based diagnostics and forensics. Surface-based approaches offer the attraction to control the conditions locally at the surface which is difficult for solution-based techniques. Moreover, they enable spatial multiplexing in an array format to produce simple and portable biosensor devices. For example, surface plasmon resonance (SPR) is a widely used technique for detecting binding events *via* changes in the local refractive index. Bartlett *et al.* reported a surface-based approach for discriminating mutations in DNA sequences using sphere segment void (SSV) substrates. SSV substrates were prepared by electrodeposition around templates made from close packed monolayers.³⁵ They are different from other solid SERS substrates such as nanotriangle surfaces or metal film on nanosphere (MFON) surfaces because the optical properties of these substrates can be tuned through the choice of sphere diameter and film thickness. Fig. 4 (top) shows SEM images of such SSV substrates together with a 3D model of the structure. Disulphide-modified oligonucleotides were immobilized on the Au surface to capture the corresponding target strand. After that the surface was incubated with mercaptohexanol in order to block bare Au surface regions and to prevent non-specific binding. Labeled target sequences

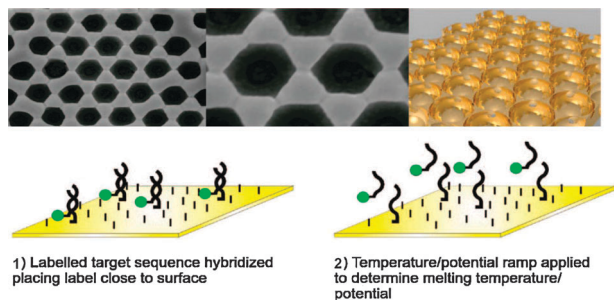


Fig. 4 DNA melting analysis of labeled target sequences hybridized to capture oligonucleotides immobilized on SSV Au substrates. From ref. 35.

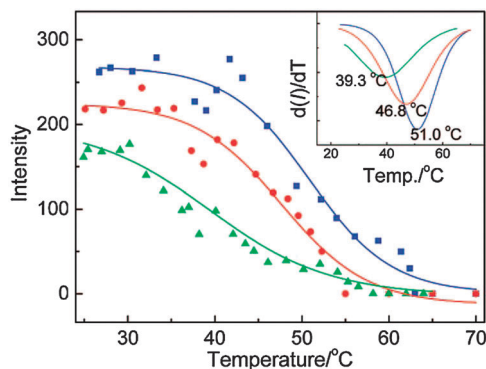


Fig. 5 Thermally induced dehybridization monitored using SERS. From ref. 35.

hybridized to the capture strand, with the label molecules located near the SSV Au surface for the efficient generation of surface-enhanced resonance Raman scattering (SERRS) (Fig. 4, bottom). In the next step, DNA melting was induced either by a temperature or a potential ramp applied to the surface.

Results of thermally induced dehybridization monitored using SERS are shown in Fig. 5. The SERS intensity of the label is plotted against temperature for three different target sequences: wild type (■, no mutation), single point mutant (●), and triple mutant (▲, triple deletion). The first derivatives of the sigmoidal fits of the intensity curves are shown in the inset (Fig. 5). The wild type exhibited the highest melting temperature at 51 °C because the sequence matches perfectly the capture sequence. The melting temperatures of the single point mutant and the triple mutant are 46.8 and 39.3 °C, respectively, demonstrating the non-perfect match due to the mutation. The presented SERS melting approach is a very sensitive method and also suitable for high throughput analysis and miniaturization; it can be potentially used in the fields of molecular diagnostics, genomics, and forensics.

3.1.2 Multiplex pathogen DNA detection using a particle-on-wire SERS sensor. A multiplexed DNA sensor can be used in various medical studies including gene profiling, drug screening, and clinical diagnostics due to its ability to provide abundant information from a small sample volume at low cost. It has been demonstrated that SERS is a powerful tool for DNA detection because of its high sensitivity and fingerprint specificity.³⁶ Recently, Kang *et al.* developed a particle-on-wire SERS sensor for multiplexed pathogen DNA detection.³⁷

Au nanowires with a diameter of ~ 150 nm were synthesized and employed as capture substrates. The surface of the Au nanowires was functionalized with thiolated capture sequences and then placed on a Si wafer. Reporter DNA sequences with Raman reporter molecules were immobilized on Au NPs. Functionalized Au nanowires on the Si substrate were incubated with target sequences, and then immersed into a suspension of the reporter DNA-functionalized Au NPs to form a Au particle-on-wire structure *via* sandwich hybridization of probe–target–reporter sequences. Thus SERS hot spots were created at the gaps between the Au nanowire and the Au NPs. Strong SERS signals from Raman reporter molecules on the reporter sequences were observed only when the complementary target sequences were added, indicating a high specificity to DNA sequences.³⁷ Target DNA concentration-dependent experiments were carried out and the results demonstrated that quantitative detection of target sequences is possible by this particle-on-wire system.

To demonstrate the multiplexing capability, DNA sequences extracted from four pathogenic strains, *Enterococcus faecium*, *Staphylococcus aureus*, *Stenotrophomonas maltophilia*, and *Vibrio vulnificus*, were used as the target sequences. A multiplexed pathogen DNA detection platform was fabricated by four Au nanowires attached to four different probe sequences, respectively, on a single Si substrate. Since the nanowires are indistinguishable, they were aligned at specific positions on the substrate for identification. A custom-built nanomanipulator was used to place the Au nanowires. The four nanowires on the substrate were incubated with various mixtures of target sequences and then with reporter sequence-functionalized Au NPs.³⁷ The results indicate that correct pathogen DNA sequences can be identified by the particle-on-wire sensor, which is a promising pathogen diagnosis method.

3.1.3 SERS detection of West Nile virus (WNV) DNA using magnetic-SERS NPs. DNA derived from the West Nile virus (WNV) genome was detected by using a combination of SERS and paramagnetic NPs (MNPs).³⁸ The MNPs were employed for capturing the target DNA, instead of flat solid substrates commonly used in conventional SERS assays for DNA detection. Separation and enrichment of the hybridized complexes was performed in a fast and convenient way by means of magnetic pull-down (Fig. 6). The MNPs were coated with an amino-functionalized silica shell by incubation with tetraethyl orthosilicate (TEOS) and 3-aminopropyltriethoxysilane (APTES). The products were incubated with NHS-PEG2-maleimide and then with the capture sequence. Au NPs were first labeled with 5,5'-dithiobis (succinimidyl-2-nitrobenzoate) (DSNB) as both the Raman reporter and the linker for the reporter sequence, and then functionalized with the reporter sequence. Fig. 6 shows the detection method for the WNV target DNA. After the formation of the hybridized complex – comprising a capture substrate, a target oligonucleotide, and a SERS label/reporter (Fig. 6) – an external magnet was used to pull down the hybridized complexes for SERS measurement. The detection limit of the WNV oligonucleotide with this method was 10 pM.

3.1.4 Separation-free DNA detection with SERS. Conventional SERS assays for hybridization-based detection of DNA sequences require time-consuming separation steps which

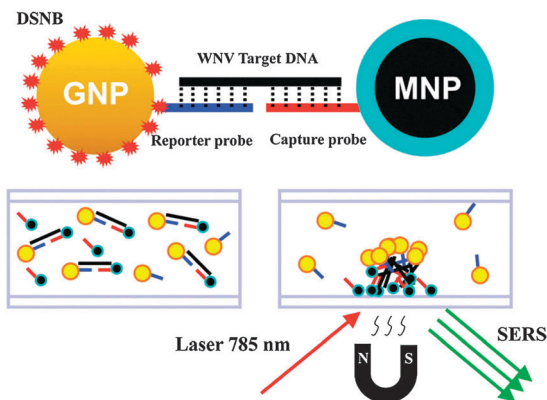


Fig. 6 SERS detection of WNV target DNA using MNPs as capture substrates. From ref. 38.

increase assay cost and also the risk of contamination. A separation-free DNA SERS detection approach has been reported recently by Graham and co-workers.³⁹ The detection relied on the difference in adsorption between double stranded (ds) and single stranded (ss) DNA to negatively charged Ag NPs. A SERS primer which contains a dye-labeled segment was rendered single-stranded upon hybridization to a target sequence.³⁹ This single-stranded segment has a higher affinity for the Ag surface than the corresponding double-stranded segment. The self-complementary region of the SERS primer has a melting temperature (40 °C) lower than the target DNA–primer duplex (62 °C). When the solution was heated above 50 °C, the primer denatured and became ssDNA. In the presence of the target sequence, the target–primer dsDNA formed before the partly self-complementary part of the primer can hybridize back when the solution was cooled, leaving a region of dye-labeled ssDNA attached. Thus strong SERS signals from the dye molecules were obtained. When non-target sequences were added, the primer formed a self-hybridized duplex with the dye molecule inside the complex, which exhibited a very low SERS response upon addition of the Ag NPs. Target and non-target DNA were therefore discriminated in a homogeneous sample without additional separation steps.

3.2 SERS immunoassays of cancer markers

3.2.1 Detection of the potential pancreatic cancer marker MUC4 in serum. Pancreatic cancer (PC) is one of the most lethal cancers and has a very poor prognosis because of the lack of a reliable tumor marker for early diagnosis.⁴⁰ For all stages combined, PC has 1- and 5-year relative survival rates of 25% and 6%, respectively. It has been found that mucin protein MUC4 is a promising biomarker for PC.⁴¹ However, detection of MUC4 in serum by enzyme-linked immunosorbent assay (ELISA) and radioimmunoassay (RIA) has not been successful. In contrast, a SERS immunoassay has been used successfully for quantitative measurements of MUC4 levels in the serum of PC patients.⁴² The key features of the immunoassay are shown in Fig. 7. A gold-coated glass slide was functionalized with dithiobis-(succinimidyl propionate) (DSP) and then incubated

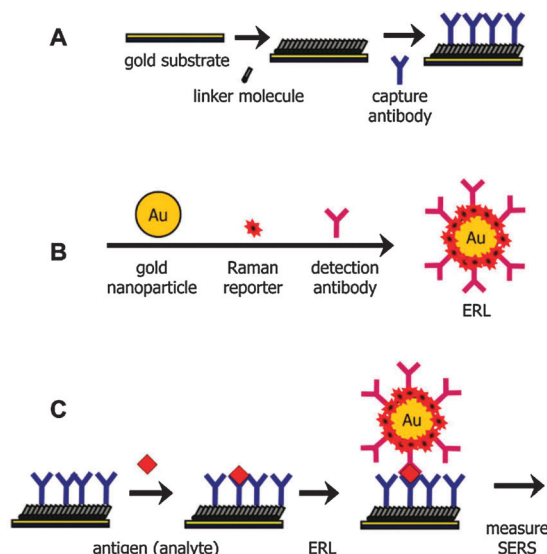


Fig. 7 SERS-based immunoassay chip design and assay scheme: (A) a capture substrate to specifically extract and concentrate antigens from solution; (B) surface-functionalized Au NPs to bind to captured antigens selectively and generate intense SERS signals; and (C) sandwich immunoassay with SERS readout. From ref. 42.

with capture antibody solution to form linkages between the amine groups on the protein and the succinimidyl ester of DSP. This slide covered with a layer of capture antibody was used as the capture substrate. Tag–antibody conjugates were prepared by incubation of Au NPs together with a mixture of DSP and 4-nitrothiophenol (4-NTP), followed by conjugation with the detection antibody. The fingerprint SERS spectra of 4-NTP were used as the readout signal of the MUC4 mucin protein in the immunoassay.

In a typical assay, capture substrates were exposed to the sample solution for 8 h in a humidity chamber. After rinsing with buffer, captured MUC4 antigens were labeled by exposition to the functionalized NPs for 16 h. The substrates were then rinsed and dried with a stream of nitrogen, and analyzed by SERS. Concentration-dependent assays for MUC4 in PBS buffer were performed. The analyte concentration was quantified using the peak intensity of the symmetric nitro stretch of NTP at *ca.* 1336 cm^{-1} . Based on these results, the SERS-based assay was used to detect MUC4 in the sera of PC patients. Five sets of pooled sera samples were analyzed after a 20-fold dilution in PBS: one pool from healthy individuals, one pool from patients with acute pancreatitis, and three pools from PC patients.⁴² The results in Fig. 8 show that sera pools from PC patients produced a significantly higher response in the SERS-based assays than the sera from normal patients and those with benign diseases. Thus, it is possible to quantitatively measure MUC4 levels in the sera for diagnostic and prognostic purposes.

3.2.2 Optoelectrofluidic sandwich SERS immunoassays. Traditional heterogeneous immunoassays always require repetitive washing steps for separating free proteins from those bound to the capture antibody. Moreover, a long incubation time is required for antibody–antigen reactions due to the diffusion of biomolecules

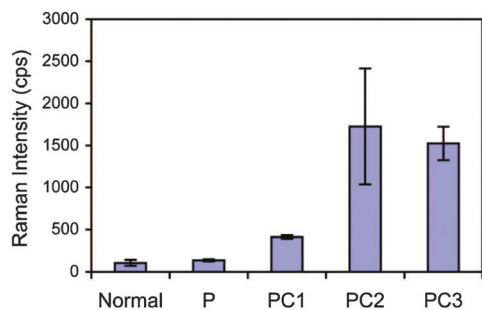


Fig. 8 SERS detection of MUC4 in pooled sera from normal individuals and patients with pancreatitis (P) or pancreatic cancer (PC1, PC2, and PC3). Each pool includes sera from 10 individuals. From ref. 42.

and functionalized NPs. Therefore, traditional SERS immunoassays, involving multiple incubation and washing steps, usually take several hours and are labor-intensive. Optoelectrofluidics based on the electrokinetic motion of particles or fluids has recently been used for a rapid and automated SERS immunoassay of alphafetoprotein (AFP).⁴³

Instead of using a flat chip as the capture substrate, polystyrene (PS) microspheres were employed for the sandwich immunoassay (Fig. 9). In contrast to conventional immunoassays on solid substrates, the immunoreaction became much faster because all the reactions occur in solution and the diffusion-limited kinetics has been overcome. For the capture of AFP antigens, the PS microspheres were functionalized with monoclonal AFP antibodies. 40 nm Ag NPs were first incubated with malachite green isothiocyanate as Raman reporter dye and then with dihydrolipoic acid for antibody conjugation. Polyclonal AFP antibody was added to NHS-activated Ag NPs to form AFP-targeted SERS labels. The AFP solution, PS microspheres, and Ag NP suspension were placed together in the sample chamber of the optoelectrofluidic device, which consists of a bare indium tin oxide (ITO) electrode and a photoconductive electrode. In optoelectrofluidics, dielectric particles with sizes ranging from hundreds of micrometres to tens of nanometres can be manipulated through dielectrophoresis (DEP) and alternating current electroosmosis (ACEO) caused by non-uniform electric fields.

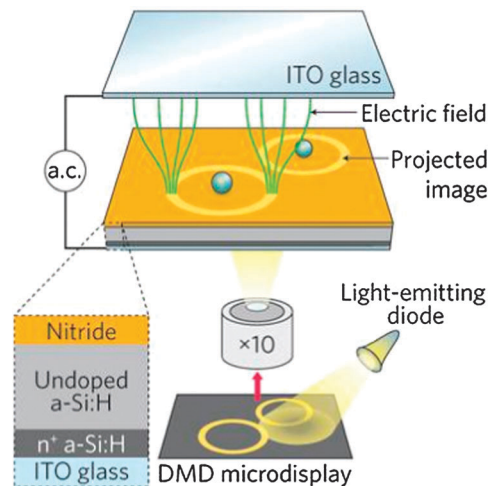


Fig. 10 Optoelectrofluidic device and internal structure. Light patterns from a programmed LCD create traps in the illuminated areas. DMD, digital micromirror device. From ref. 44.

The non-uniform electric fields can be created by optical image-controlled 'virtual electrodes' in the optoelectrofluidic device (Fig. 10).⁴⁴ After the sample injection, all the steps were automatically controlled by an applied ac signal and a programmed LCD image, including mixing of the samples, washing of free analytes and probing NPs, and local concentration of the immunocomplexes. SERS signals were recorded from the locally concentrated immunocomplexes. The assay required only 500 nL sample (AFP solution), the detection limit was 98 pg mL^{-1} , and the assay required only ~ 5 minutes after sample injection.

3.2.3 Lab-on-a-bubble SERS immunoassay for cholera. Buoyant silica bubbles were employed as capture substrates in a cholera SERS immunoassay.⁴⁵ For preparation of the capture substrates, the silica bubbles were silanized with APTES and then functionalized with anti-cholera toxin (CT) antibody. 50 nm Au NPs were used as SERS substrates. The freshly prepared NPs were labeled with 1,2-bis(2-pyridyl) ethylene (BPE), coated with a silica shell, and then incubated with the anti-CT antibody solution to allow antibodies to

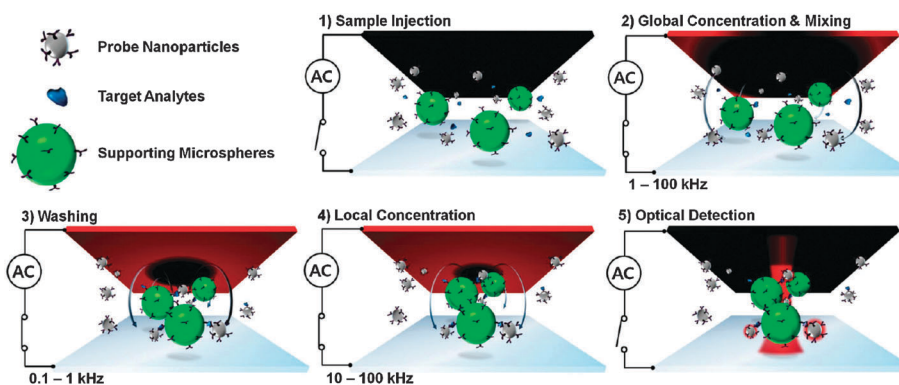


Fig. 9 The Raman probe-tagged metallic NPs bind onto the supporting microspheres in the medium of target analytes, forming an immunocomplex. All processes, including sample concentration, mixing, reaction, and washing, are automatically conducted by a programmed LCD. The final step is the SERS detection of the immunocomplexes. From ref. 43.

adsorb on the silica-coated Au NPs. After that recombinant β subunit CT antigen was incubated with the capture bubbles and functionalized Au NPs to form the sandwich immunocomplex. Buoyancy could pull the immunocomplexes from the sample solution to a compact monolayer of bubbles on the surface of the sample. Following the incubation, the entire reaction suspension was transferred to a polished aluminum surface where the bubbles were allowed to rise to the surface in about 5 minutes.⁴⁵ SERS was collected from the monolayer of the bubbles on top of the sample volume. The BPE marker peak at $\sim 1600\text{ cm}^{-1}$ was normalized against the glass fluorescence peak from the silica bubbles at $\sim 1000\text{ cm}^{-1}$ to establish an internal standard. The limit of detection was 1100 ng, which is volume-independent because of the enrichment of the analyte when the bubbles were concentrated on top of the liquid sample.

3.3 Detection and imaging of biological cells using SERS labels

3.3.1 pH-sensitive plasmonic vesicles for cancer cell targeting and drug delivery.

Polymeric vesicles are intriguing drug delivery carriers because of their robust structures and versatile chemical functionality. Duan and co-workers have recently reported the development of plasmonic vesicles assembled from amphiphilic Au NPs for cancer-targeted drug delivery, which can be tracked by plasmonic imaging and SERS.⁴⁶ 14 nm Au NPs were first coated with 2-(4-(bis(4-(diethylamino)phenyl)(hydroxymethyl)phenoxy)ethyl 5-(1,2-dithiolan-3-yl)pentanoate (BGLA) as Raman reporter molecules. Then two different polymer brushes, a hydrophobic copolymer comprising methyl methacrylate and 4-vinylpyridine (PMMAVP) together with hydrophilic poly(ethylene glycol) (PEG), were grafted on the Au NPs. In this step, thiolated PEG and 2,2'-dithiobis[1-(2-bromo-2-methylpropionyloxy)]ethane (DTBE), an atom transfer radical polymerization (ATRP) initiator, were immobilized on the Au surface. Then PMMAVP brushes were grown on the functionalized NPs through surface-initiated ATRP.⁴⁶ The obtained amphiphilic Au NPs were assembled into plasmonically active vesicles *via* rehydration of the film.⁴⁷ Fig. 11 shows TEM and SEM images of the vesicles. The 4VP in the hydrophobic PMMAVP brush has a pK_a of 5.4, below which the copolymer becomes water-soluble due to the protonation of pyridine groups. Therefore in an acidic environment, destruction of the vesicles was observed, which enabled both pH-triggered drug release and *in situ* SERS/plasmonic monitoring of pH.

Doxorubicin (DOX) was used as a model drug for the intracellular drug delivery. DOX molecules were loaded in the plasmonic vesicles by a modified film-rehydration method, in which DOX deprotonated by an equivalent of triethylamine was dissolved in chloroform and co-deposited with the amphiphilic Au NPs to form the film for rehydration.⁴⁶ The vesicles were conjugated with monoclonal antibodies to HER2 proteins *via* carboxylic groups from the heterofunctional PEG in the thiolated PEG chains. The antibody-conjugated vesicles were incubated with HER2-positive SKBR-3 breast cancer cells for cancer cell targeting and drug release. It is important to mention that the dramatic changes in the scattering properties

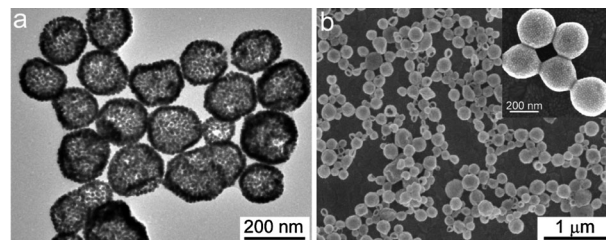


Fig. 11 TEM (a) and SEM (b) images of the pH-sensitive plasmonic vesicles assembled from 14 nm gold NPs with mixed PEG and PMMAVP brushes. From ref. 46.

and SERS intensity of the plasmonic vesicles as well as the drug release occur in response to the same pH trigger, which is highly relevant to the acidic environment of endocytic compartments.⁴⁶ After the functionalized vesicles bind to the target cell surface, receptor-mediated cellular uptake of the vesicles was observed, which caused the dissociation of the vesicles and release of DOX when the organelles evolved from early endosomes (pH 5.9–6.2) to late endosomes/lysosomes (pH 4.7–5.5). The whole process could be tracked by SERS due to the strong plasmonic coupling of the Au NPs in the vesicles and SERS intensity decrease accompanied by the drug release.

3.3.2 Identification of breast cancer stem cells using SERS.

It has been found that breast cancer cells expressing the CD44 antigen and not the CD24 antigen ($CD44^+/CD24^-$) exhibit enhanced invasive properties.⁴⁸ These two cell surface markers were detected using SERS in three breast cancer cell lines, MCF-7, MDA-MB-231, and MDA-MB-468, to identify a $CD44^+/CD24^-$ subpopulation of cancer stem cells (CSC).⁴⁹ Pointer NPs functionalized with antibodies specific to CD24 or CD44 and different DNA sequences were used to target these two surface markers. Enhancer NPs conjugated with corresponding complementary DNA sequences and Raman reporter molecules were employed to form a network structure around the pointer NPs that can be detected by SERS. 4-Mercaptopyrindine (4-MP) and 4,6-dimethyl-2-pyrimidinethiol (DMPT) were used as reporters for CD44 and CD24, respectively. For the SERS detection, fixed cancer cells were first incubated with pointer NPs to localize the particles at corresponding membrane marker sites due to the antibody–antigen recognition. Then the enhancer NPs were added to form the hybridization network structure at the corresponding marker sites targeted by the pointer particles. SERS mapping of two different Raman reporters, 4-MP (characteristic peak at 1094 cm^{-1}) and DMPT (characteristic peak at 569 cm^{-1}) representing CD44 and CD24, respectively, was conducted to assess the distribution of corresponding surface markers on selected cancer cells.⁴⁹ The results indicated that MDA-MB-231 cells express the CD44 antigen and not the CD24 antigen ($CD44^+/CD24^-$ subpopulation).

3.3.3 Multiplexed detection of bronchioalveolar stem cells with F-SERS dots.

SERS has the capability to detect multiple target molecules due to the small line width of vibrational Raman bands. This ability for multiplexed detection can be further improved when fluorescence is used together with SERS. Fluorescent-SERS (F-SERS) dots were synthesized and

used for detection and differentiation of three cellular proteins – CD34, Sca-1, and SP-C – on bronchioalveolar stem cells (BASC).⁵⁰ Silica NPs of ~120 nm size were used as templates for the synthesis of the F-SERS dots. The surface of the silica particles was first functionalized with thiol groups using (3-mercaptopropyl) trimethoxysilane (MPTMS). Then Ag was deposited on the surface by reduction of AgNO₃ in the silica particle suspension. Raman reporter molecules including mercaptotoluene (MT), benzenethiol (BT), and naphthalenethiol (NT) were added to the colloid. The Raman reporter-functionalized assemblies (silica core/silver satellites) were treated with sodium silicate and subsequently with a mixture of fluorescein isothiocyanate (FITC)-3-aminopropyltriethoxysilane (APTES) conjugate and tetraethylorthosilicate (TEOS), resulting in a fluorescent layer outside. The obtained F-SERS dots were functionalized with carboxyl groups and then conjugated with monoclonal antibodies against CD34, Sca-1, and SP-C. After the incubation of the cells with the SERS-labeled antibodies, SERS mapping was carried out using the intensities of marker bands at 1593 cm⁻¹ for MT, 997 cm⁻¹ for BT, and 1378 cm⁻¹ for NT, in order to determine the spatial distribution of CD34, Sca-1, and SP-C, respectively. CD34 and Sca-1 were detected on the cell surface, while SP-C was only expressed in the cytoplasm. The fluorescence signal is important when the cells are located in complex biomedical systems. For example, fast and effective localization of the BASC in tissue sections can be easily achieved by the fluorescence signal from the F-SERS dots before the SERS multiplex detection of the different marker proteins.

3.3.4 SERS monitoring of photothermal therapy response of cancer cells. Au NPs of different sizes and shapes with SPR peaks in the near-infrared (NIR) region, such as Au nanorods and nanowires, can be used for hyperthermic destruction of cancer cells. Ray *et al.* reported SERS monitoring of photothermal therapy on prostate cancer cells by using popcorn-like Au NPs.⁵¹ These NPs have an extinction band at 580 nm, *i.e.*, the plasmon resonance cannot be excited by the NIR radiation. However, when they were functionalized with targeting molecules and attached on the cancer cells, a broad extinction band due to the aggregation of the NPs appeared in the NIR region and facilitated the photothermal treatment. Spherical Au seeds were produced by reduction of HAuCl₄ with NaBH₄ in the presence of sodium citrate. Then ascorbic acid was added as a reducing agent in the presence of CTAB as a shape-templating surfactant and Au nanopopcorns were formed. The particles were functionalized with two targeting biomolecules, A9 RNA anti-prostate-specific membrane antigen (PSMA) aptamer and monoclonal anti-PSMA antibody, to increase the binding efficiency of the NPs on the LNCaP human prostate cancer cells. Rhodamine 6G (Rh6G) modified on the RNA aptamer was used as a Raman reporter for SERS measurement.

After incubation with the LNCaP cells, the NPs formed large aggregates on the cell membrane, leading to a plasmon peak in the NIR. Photo-thermal treatment of the cells was performed with 785 nm continuous-wave radiation. SERS detection was carried out by using 670 nm laser excitation. Fig. 12a shows the linear relationship between the percentage of LNCaP cell

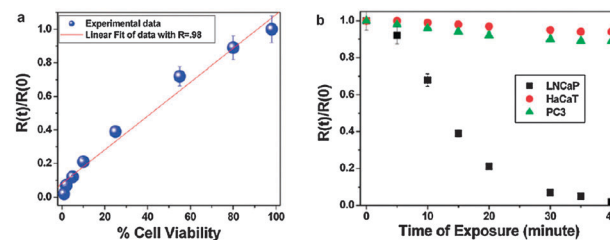


Fig. 12 Relationship between SERS intensity change and LNCaP cell viability when the cells were exposed to 100 mW, 785 nm radiation for 30 min (a) and photothermal therapy effect on different cell lines at different exposure times (b). From ref. 51.

viability and the SERS intensity change. The decrease of the SERS intensity was attributed to the breaking of the S–Au bond between the Au NPs and the Rh6G-modified A9 RNA aptamer caused by the strong photothermal effect.⁵¹ This change was not observed when the target cells were absent: in this case no aggregates were formed and the plasmon resonance at 580 nm could not be excited by the NIR laser radiation. Fig. 12b shows the change in SERS intensity at different radiation times during the photothermal treatment of LNCaP, PC-3, and HaCaT cells, indicating that the method is highly selective.

3.3.5 Detection of circulating tumor cells in blood. SERS labels can be used to detect cancer cells in the presence of human whole blood, which is a promising method for cancer diagnosis. The breast cancer cell line SKBR3 with human epidermal growth factor receptor-2 (her2) highly expressed on the surface was used as a model target.⁵² SERS labels were prepared by silica encapsulation of Au-NPs coated with a submonolayer of Raman reporter molecules. The silica surface was functionalized with anti-HER2 antibodies for targeted binding to the model tumor cell. A magnetic particle, comprising a magnetic bead and epithelial cell-specific antibodies (epithelial cell adhesion molecule, anti-EpCAM) immobilized on the surface, was used to capture the target cell. The breast cancer cell originates from the epithelium so that the capture particle will specifically bind to this tumor cell, but not to normal circulating blood cells. After incubation of the SKBR3 cells with the capture particles and the SERS labels, the reaction tube was placed by a magnet to concentrate the magnetic beads along with captured cells to a specific position on the side of the tube where the SERS signal was collected. The limit of detection was less than 10 cells per mL in buffer solution. For the blood test, the cancer cells were spiked directly into whole blood prior to the incubation with capture particles and SERS labels. After magnetic enrichment, the SERS signal was obtained directly in whole blood without washing or other handling steps. The limit of detection in blood is about 50 cells per mL. However, the concentration of circulating tumor cells in blood of patients is usually less than 10 cells per mL.⁵³ This limit of detection therefore needs further improvement to be used in clinical detection.

3.4 Medical SERS studies on tissue specimens

3.4.1 SERS microscopy for protein localization in tissue sections. Detection and localization of prognostic markers in tissues is central for cancer diagnostics. SERS has great

potential to be used in this area due to its multiplexing capabilities, quantification, photostability and improved image contrast by red to NIR laser excitation. The proof-of-concept for immuno-SERS microscopy^{10,54} demonstrated the selective localization of prostate-specific antigen (PSA) in a prostate tissue specimen by a SERS-labeled anti-PSA antibody. In the past few years, various SERS labels comprising different metals, sizes and shapes as well as different Raman reporter molecules have been used for tissue imaging. Recently, hydrophilically stabilized Au nanostars with ethylene glycol-modified aryl thiols as Raman reporter molecules were employed for immuno-SERS microscopy on prostate tissue.⁵⁵

Au nanostars were employed because of their high plasmonic activity at the tips and their plasmon peak in the red, which results in low autofluorescence from the biological samples upon red laser excitation. TEM images of several ~ 60 nm gold nanostars, a single gold nanostar and one of its tips at higher magnification are shown in Fig. 13.⁵⁵ 10 nm Au seeds were first mixed with glycerol. After that a mixture of sodium citrate, AgNO₃, and HAuCl₄ was rapidly added, immediately followed by the addition of hydroquinone solution. Surface functionalization of gold nanostars was achieved by incubation with Raman reporter molecules which yield a complete SAM on the particle surface. The reporter molecules comprise terminal hydrophilic ethylene glycol spacers, which stabilize the SERS particles and improve their water solubility. A small portion of the stabilized Raman reporters (1%) has a terminal carboxyl group for subsequent bioconjugation (here to anti-p63 antibody).

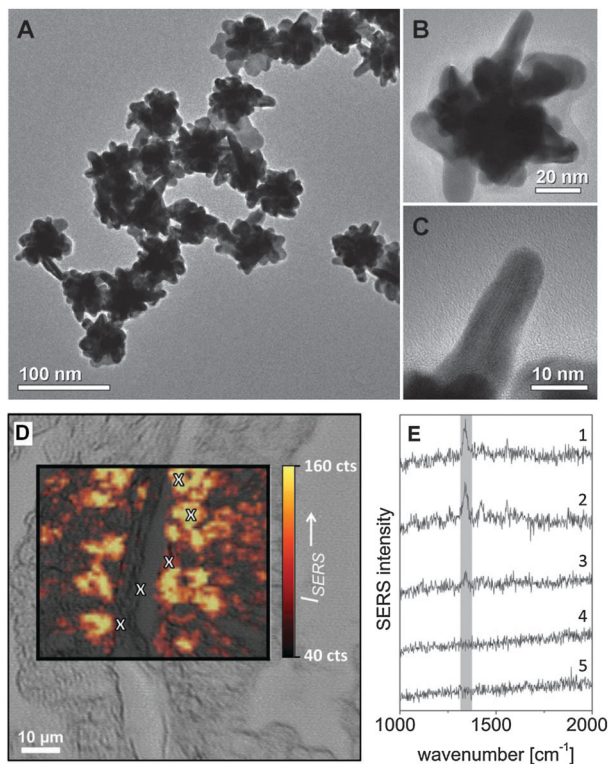


Fig. 13 Immunohistochemistry with hydrophilically stabilized gold nanostars as SERS labels, conjugated to antibodies directed against p63. From ref. 55.

Benign prostate tissue sections were incubated with the anti-body-functionalized nanostars. Fig. 13D shows the SERS mapping of the incubated tissue. A white light image of the prostate tissue section was overlaid with the corresponding SERS false color image based on the intensity of the Raman marker band of the SERS label at *ca.* 1340 cm⁻¹ (Fig. 13E). The signature of the SERS label was only observed in the basal epithelium, but not in the stroma/connective tissue or lumen. These results indicate the selective abundance of p63 in the basal cells of the benign prostate.

3.4.2 SERS detection/imaging in deep tissue. SERS measurements in deep tissue by NIR excitation have great potential to be used for rapid *in vivo* diagnosis, including early cancer detection/staging and treatment monitoring. Conventional confocal techniques can probe depths up to 200 μ m with non-SERS particles. Stone *et al.* reported surface-enhanced spatially offset Raman spectroscopy (SESORS) for detecting NPs deeply buried in tissue.⁵⁶ Transmission Raman spectroscopy was used to collect SERS from the opposite side of the sample (Fig. 14). Ag NPs labeled with reporter molecules were injected into the center of fresh porcine tissue. SERS from these Ag NPs was obtained by SESORS. More recently, multiplexed detection and imaging of molecule-specific SERS particles deeply buried in tissue was developed.⁵⁷ Four different Raman reporter molecules were immobilized on the NP for multiplexed SERS readout. Each NP suspension was injected into one of the corners of a 10 mm square, from where multiplexed SESORS imaging of the NPs was obtained according to the characteristic bands of the four reporter molecules.

3.5 SERS *in vivo* detection

3.5.1 *In vivo* tumor targeting and SERS detection. Targeting and detection of tumors in live animals has been achieved by using antibody-conjugated Au nanoprobe and SERS.⁵⁸ For preparation of the nanoprobe, Au NPs were first modified with the Raman reporter 3,3'-diethylthiatricarbocyanine (DTTC) and then stabilized by thiol-modified polyethylene glycols (PEG). These PEGylated SERS nanoprobe were even more sensitive than fluorescent NIR quantum dots. Single-chain variable fragment (ScFv) antibodies were conjugated to hetero-functional PEG (HS-PEG-COOH) to recognize the epidermal growth factor receptor (EGFR), which is overexpressed in many types of

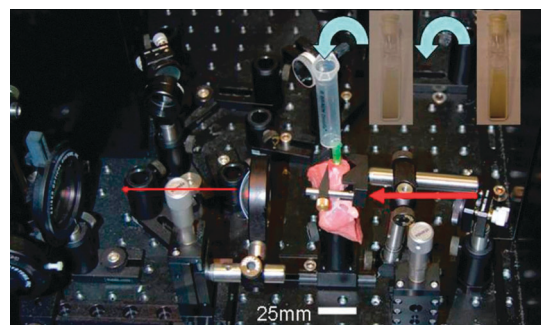


Fig. 14 Transmission Raman apparatus with arrows indicating illumination and inelastic scattering collection. From ref. 56.

malignant tumors. The resultant nanoprobes were then injected into nude mice bearing human head-and-neck squamous cell carcinoma (Tu686) xenograft tumor for *in vivo* SERS detection. The results demonstrated specific recognition and spectroscopic detection of EGFT-positive tumor in animal models.

3.5.2 *In vivo* detection of inflammation by SERS. Detection of inflammation is important for the diagnosis and treatment of autoimmune, infectious, and metastatic diseases. SERS *in vivo* detection of intercellular adhesion molecule 1 (ICAM-1) was performed by using SERS labels injected into live mice.⁵⁹ Au NPs modified with Raman reporter molecules were encapsulated with a silica shell and then conjugated to anti-ICAM-1 antibody to target ICAM-1 expressed in mice. ICAM-1 expression was induced by local lipopolysaccharide (LPS) injection in mouse ear pinnae. Approximately 24 h after the intradermal LPS injections, intravenous injection of the SERS labels was performed. SERS spectra were measured 30 minutes after the injection of the nanotags. SERS spectra recorded from ears of mice injected with anti-ICAM-1 NPs reproduced spectral features corresponding to the neat SERS labels. Fluorescent detection of ICAM-1 by using anti-ICAM-1-fluorescein isothiocyanate (FITC) was performed under the same condition as the SERS measurement. The results indicated that SERS labels produce higher sensitivity detection of ICAM-1 compared with conventional fluorophore-antibody conjugates and offer improvements in terms of depth resolution and signal-to-noise ratio.

3.5.3 Bifunctional MRI-SERS NPs for imaging in living mice. Bifunctional NPs comprising a superparamagnetic material and a plasmonic metal can be used in both magnetic resonance imaging (MRI) and SERS. Medarova and co-workers synthesized Au-iron oxide hybrid NPs by growing Au on iron oxide NPs.⁶⁰ First, citrate reduction of HAuCl_4 doped small Au NP seeds on the iron oxide particle surface. These seed particles were further enlarged by hydroxylamine reduction of HAuCl_4 in the suspension. Then the Raman reporter molecule 3,3'-diethylthiatricarbocyanine (DTTC) was added for adsorption onto the Au surface. PEG was used to prevent aggregation of the NPs and to keep the Raman-active dyes on the surface by forming a protective shell. T2-weighted magnetic resonance images showed that the signal intensity of the obtained bifunctional hybrid particles was comparable to iron oxide NPs and visibly lower than Au NPs because superparamagnetic iron oxides shortened the transverse (T_2) relaxation time of surrounding protons. The bifunctional NPs were injected into the muscle of a living mouse for *in vivo* MRI and SERS detection. Fig. 15A–C shows the results from the MRI experiment. As a control, the area at which Au NPs were injected appeared bright (Fig. 15B left), due to edema, which has a higher T_2 value than surrounding muscle. In contrast, an area of signal loss was observed due to bifunctional NP injection (Fig. 15B right), which is an indication of contrast agent accumulation. SERS detection was performed directly in the injection area (Fig. 15D). Both spectra from the living mouse and excised muscle tissue (excised after *in vivo* detection) showed the same spectral feature as the DTTC SERS spectrum obtained in solution.

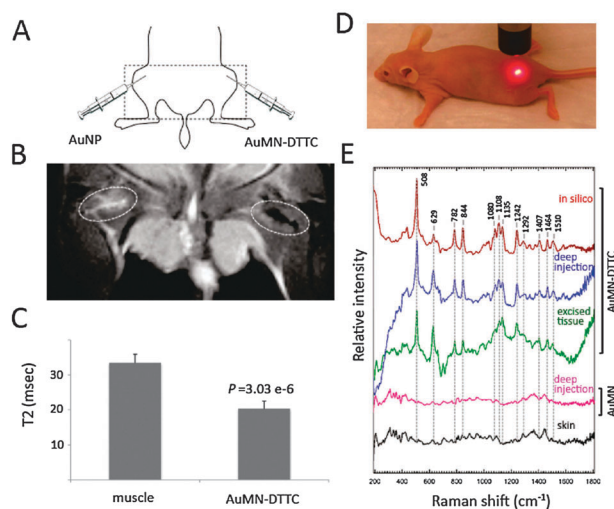


Fig. 15 *In vivo* MRI/SERS study on nude mice by using Au-iron oxide bifunctional NPs. From ref. 60.

3.5.4 Triple-modality MRI-photoacoustic-SERS NPs for brain tumor imaging. Delineation of brain tumor margins is very important for better outcomes of patients with brain tumors. Gambhir and co-workers have recently reported triple-modality MRI-photoacoustic-Raman imaging (MPR) which can help to delineate the margins of brain tumors in living mice.⁶¹ The MPR NP contains a 60 nm Au core modified with *trans*-1,2-bis(4-pyridyl)-ethylene as the Raman reporter molecule. Then the SERS-active particle was coated with a 30 nm thick silica shell. After that, the Au-silica core-shell NP was further modified with 1,4,7,10-tetraazacyclododecane-1,4,7,10-tetraacetic acid (DOTA)- Gd^{3+} , resulting in a silica encapsulated Au NP with Gd^{3+} on the surface. After subcutaneous injection of these MPR NPs into nude mice, the MRI, photoacoustic and SERS signal *in vivo* correlated well to the MPR concentration ($R^2 = 0.99, 0.97$ and 0.99 for MRI, photoacoustic and SERS, respectively).

The MPR NPs were then used to visualize brain tumor in living tumor-bearing mice by injection through tail vein. It's notable that the NPs do not carry any tumor targeting biomolecules. The authors hypothesized that the NPs would enter the extravascular space by diffusion through the disrupted blood-brain barrier and accumulate in cells within the brain tumor because of enhanced permeability and retention (EPR) effect.⁶¹ The MPR NP signal can facilitate the tumor resection *in vivo*. The tumor-bearing mice were placed under general anesthesia and craniotomies and subsequent *in vivo* SERS imaging were performed. Then sections of the detected brain tumor were removed using visual inspection. High-resolution intraoperative SERS images were obtained after each resection step and correlated with the intraoperative photographs (Fig. 16). Several small foci of residual SERS signal (Fig. 16b) were found in the resection bed after the tumor resection seemed to be complete by visual inspection. Then the resection was extended to include these foci located near the tumor-brain interface. Histological analysis of this tissue indicates frequent finger-like microscopic extensions of the

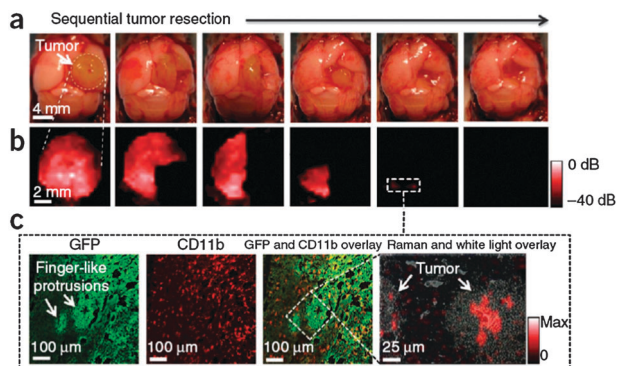


Fig. 16 SERS-guided intraoperative surgery using MPR NPs. From ref. 61.

tumor into the surrounding brain tissue (Fig. 16c). Thus with the MPR NP accumulation in the tumor it is possible to detect cancerous foci which are not visible to the naked eye.

3.5.5 *In vivo* SERS-based cancer detection using highly sensitive Raman reporters. One of the major bottlenecks in SERS *in vivo* detection is the development of NIR-sensitive Raman reporters. Most of the commonly used Raman reporter dyes such as crystal violet and rhodamine 6G are active in the visible region. For *in vivo* detection, it is important that the Raman reporter is active in the NIR region. For example, the cyanine derivative DTTC has been regarded as a standard Raman reporter in NIR SERS/SERRS studies. However, the signal intensity from DTTC is moderate. Samanta *et al.* reported the synthesis of tricyanocyanine derivatives with NIR absorption properties and ultrasensitive SERS *in vivo* cancer detection.⁶² A series of compounds were obtained and the SERS intensity of them was compared by using 60 nm Au NPs as the SERS substrate. CyNAMLA-381, which displayed about 12-fold higher sensitivity than the standard DTTC, was chosen as the best Raman reporter among them (Fig. 17). SERS probes with this reporter molecule were prepared for *in vivo* cancer detection. The Raman reporter-modified Au NPs were protected with bovine serum albumin (BSA) and glutaraldehyde to prevent NP aggregation and desorption of the reporter molecules. Then the particles were functionalized with HER2-recognition antibodies (anti-HER2 monoclonal antibody or scFv anti-HER2 antibody). The obtained nano-probes were injected into nude mice bearing xenografts generated from SKBR-3 cells. After 5 hours, SERS spectra from the tumor site perfectly resembled the SERS spectra of the nano-probes.

3.5.6 *In vivo* detection using SERS-active acupuncture needles. Although *in vivo* SERS detection in animal models has attracted great interest in the past few years, clinical diagnosis remains challenging because metal NPs are required for signal enhancement. Since the long-term toxicity of metal NPs inside the human body is not understood, injection of suspended NPs into patients should be avoided. Acupuncture needles, which provide minimally invasive merits including no bleeding and mitigation of pain, have been employed for medical treatments for several thousand years. Dong *et al.* reported the use of

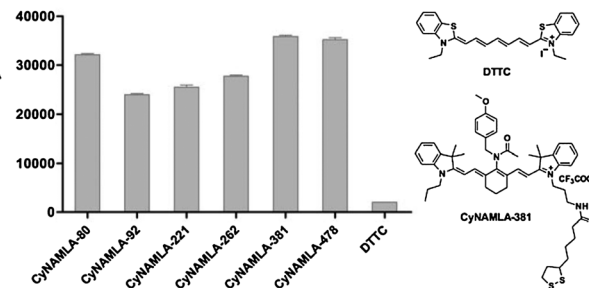


Fig. 17 SERS intensity of some tricyanocyanine derivatives on 60 nm Au NPs obtained using 785 nm excitation. From ref. 62.

acupuncture needles as a carrier of SERS-active NPs for *in vivo* detection. After the SERS-active needle was inserted into the body, interstitial fluids would diffuse into the gaps between the attached NPs; after the needle was pulled out, analytes in the fluids diffused into the particle gaps at different depths were taken out for SERS measurement.⁶³ To fabricate the SERS-active needles, commercial stainless-steel acupuncture needles of 200 μm in diameter were first incubated with 3-mercaptopropyl triethoxysilane (MPTES). Then the SERS-active NPs, comprising a thin Au shell coated on a dielectric core, were assembled on the needle surface (Fig. 18). The ability of *in vivo* SERS detection of the needles for drug molecules was assessed by using 6-mercaptopurine (6-MP) as a model drug, which is one of the major drugs for acute lymphoblastic leukemia. 6-MP aqueous solution was injected into the ear vein of a New Zealand rabbit. After that two SERS-active needles were inserted into the other ear vein and vastus lateralis tendon to detect the drug concentration in blood and muscles, respectively. SERS measurement was carried out immediately after the needle was pulled out. The results indicated that the concentration of free 6-MP in the body decreased after injection, and the concentration of 6-MP in blood is higher than that in muscles.

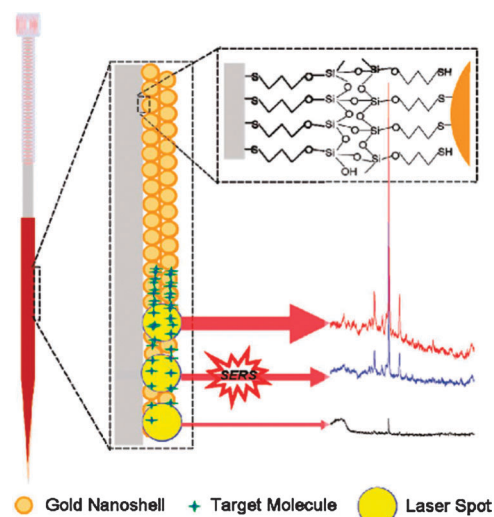


Fig. 18 Illustration of the structure of a SERS-active needle and its working principle. From ref. 63.

3.6 Detection schemes based on SERS labels: a critical perspective

The physicochemical properties of Au or Ag NPs, which are usually employed to make SERS labels, are strongly size- and shape-dependent. Typically, only NPs larger than 20 nm have sufficient plasmonic activity and provide the required SERS enhancement.^{64,65} SERS labels are therefore much bigger and heavier than other molecule-based labels (*i.e.* fluorescent and isotope labels) used in medical studies. Thus, SERS label/ligand-conjugates may exhibit poorer target binding specificities and penetration abilities in a biomedical environment, especially in biological cells (see Section 3.3) and in tissues (see Section 3.4). However, conclusive experimental demonstration of these aspects for SERS NPs is missing in the literature. Nevertheless, SERS labels with smaller size and/or less weight should be developed to circumnavigate this (potential) problem. For instance, a dimer of two 30 nm Au NPs has a higher SERS enhancement but 4 times less weight than a single 60 nm Au NP.⁶⁶ Another important issue for the use of SERS labels in medical applications is the cytotoxicity of metal NPs. Although Au is an inert metal in the biomedical system, the cytotoxicity of Au NPs is not clear until now.^{67–69} A further problem is the biodistribution of metal NPs in the human body. If the metal NPs cannot be removed completely from the patients after the medical treatment, the SERS labels may (should?!) not be introduced into the patients. Thus SERS labels may only better be used *in vitro* (blood and urine tests, for example) until these toxicity and biodistribution issues have been resolved.

4. Perspectives

SERS has become a mature vibrational spectroscopic technique over the last decades and the number of applications in medical studies is rapidly increasing. SERS is quite different from other spectroscopic methods used in medical applications such as fluorescence and UV/Vis absorption spectroscopy. First, SERS provides abundant molecular structural information directly from the sample when used in the label-free approach. Second, SERS provides fingerprint information for different molecules which increases the detection specificity. Third, SERS has narrow bands and thus avoids spectral overlap in multiplexed detection schemes. These advantages make SERS a very attractive technique for molecular diagnostics.

In this perspective article, some recent medical applications of SERS are summarized. In general, SERS can be used in two different modalities, depending on how the SERS signal correlates with chemical information from the sample. One modality is the label-free detection. In this case the SERS spectrum obtained from the analyte can be used to obtain structural information, to identify analytes and to determine its concentration.^{70–72} Label-free SERS detection is usually limited to molecules with surface-seeking groups since only molecules on or near the metal surface experience the necessary enhancements upon excitation. However, the majority of molecules involved in medical studies do not have any surface-seeking

group. Therefore label-free detection of target molecules without surface-seeking groups will significantly expand the medical application of SERS.

The second modality is the use of SERS labels for detection and imaging of target biomolecules in medical samples.^{73–75} Although the spectrum obtained here is just used for readout purpose without the aim to gain any chemical or structural information on the target itself, the SERS labels provide strong and fingerprint signal which is more sensitive and reliable than label-free detection, especially for biomolecules in a complex biological system. Quantitative detection, which requires both high sensitivity and high reproducibility, is one of the central tasks in medical applications of SERS labels. Unfortunately, there seems to be an unresolvable conflict between reproducibility and sensitivity in SERS, partly due to poor structural reproducibility of metallic nanostructures with high plasmonic activity. Synthesis of monodisperse and stabilized SERS particles with highly efficient plasmonic activity will definitely help to solve this conflict. For example, NP dimers or trimers can be created *via* various aggregation methods and purified with various separation methods including density gradient centrifugation.^{66,76} Also plasmonic superstructures are promising candidates in medical studies.^{77,78} On the other hand, Raman reporter molecules with absorption in the NIR need to be developed since NIR excitation is more suitable for medical studies because of low background fluorescence, minimal radiation damage and deep tissue penetration in this region. These surface-enhanced resonance Raman scattering (SERRS)-active reporters will further increase the detection sensitivity in medical applications.⁶²

Finally, before the injection of colloids into a patient, possible toxicological effects of metal NPs on patients including their biodistribution must be considered. Maybe *in vivo* targeting using SERS labels will not be performed clinically in the near future, unless the NPs can be removed after the measurement, or the long-term toxicity of Au NPs in the body has been thoroughly understood. Nevertheless, SERS detection without the need to inject colloidal NPs, such as the use of SERS-active needles,⁶³ has already exhibited potential advantage for *in vivo* applications. In any case, the exciting developments during the last few years are very promising and the coming years will help to more clearly identify those areas in which SERS can provide information which other techniques such as fluorescence or MRI cannot offer.

Acknowledgements

This work was supported by the Alexander-von-Humboldt Foundation and the Deutsche Forschungsgemeinschaft (DFG).

References

- 1 A. Otto, *J. Raman Spectrosc.*, 1991, **22**, 743–752.
- 2 P. L. Stiles, J. A. Dieringer, N. C. Shah and R. P. Van Duyne, *Annu. Rev. Anal. Chem.*, 2008, **1**, 601–626.

- 3 K. Kneipp, H. Kneipp, I. Itzkan, R. R. Dasari and M. S. Feld, *J. Phys.: Condens. Matter*, 2002, **14**, R597–R624.
- 4 *Surface-Enhanced Raman Spectroscopy: Analytical, Biophysical and Life Science Applications*, ed. S. Schlücker, Wiley-VCH, Weinheim, Germany, 2011.
- 5 K. N. Heck, B. G. Janesko, G. E. Scuseria, N. J. Halas and M. S. Wong, *J. Am. Chem. Soc.*, 2008, **130**, 16592–16600.
- 6 W. Xie, C. Herrmann, K. Kömpe, M. Haase and S. Schlücker, *J. Am. Chem. Soc.*, 2011, **133**, 19302–19305.
- 7 V. Joseph, C. Engelbrekt, J. D. Zhang, U. Gernert, J. Ulstrup and J. Kneipp, *Angew. Chem., Int. Ed.*, 2012, **51**, 7592–7596.
- 8 N. Leopold, M. Haberkorn, T. Laurell, J. Nilsson, J. R. Baena, J. Frank and B. Lendl, *Anal. Chem.*, 2003, **75**, 2166–2171.
- 9 E. A. Carrasco, M. Campos-Vallette, P. Leyton, G. Diaz, R. E. Clavijo, J. V. Garcia-Ramos, N. Inostroza, C. Domingo, S. Sanchez-Cortes and R. Koch, *J. Phys. Chem. A*, 2003, **107**, 9611–9619.
- 10 S. Schlücker, *ChemPhysChem*, 2009, **10**, 1344–1354.
- 11 J. Kneipp, H. Kneipp and K. Kneipp, *Chem. Soc. Rev.*, 2008, **37**, 1052–1060.
- 12 B. Panchapakesan, B. Book-Newell, P. Sethu, M. Rao and J. Irudayaraj, *Nanomedicine*, 2011, **6**, 1787–1811.
- 13 E. Boisselier and D. Astruc, *Chem. Soc. Rev.*, 2009, **38**, 1759–1782.
- 14 D. Drescher and J. Kneipp, *Chem. Soc. Rev.*, 2012, **41**, 5780–5799.
- 15 X. Q. Chi, D. T. Huang, Z. H. Zhao, Z. J. Zhou, Z. Y. Yin and J. H. Gao, *Biomaterials*, 2012, **33**, 189–206.
- 16 M. Knauer, N. P. Ivleva, X. J. Liu, R. Niessner and C. Haisch, *Anal. Chem.*, 2010, **82**, 2766–2772.
- 17 R. Tian and J. S. Ingwall, *Circulation*, 2008, **117**, 1772–1774.
- 18 S. G. Obican, R. H. Finnell, J. L. Mills, G. M. Shaw and A. R. Scialli, *FASEB J.*, 2010, **24**, 4167–4174.
- 19 E. H. Reynolds, *Lancet*, 1967, **1**, 1086.
- 20 W. Ren, Y. X. Fang and E. K. Wang, *ACS Nano*, 2011, **5**, 6425–6433.
- 21 K. Ock, W. I. Jeon, E. O. Ganbold, M. Kim, J. Park, J. H. Seo, K. Cho, S. W. Joo and S. Y. Lee, *Anal. Chem.*, 2012, **84**, 2172–2178.
- 22 C. J. Choi, H. Y. Wu, S. George, J. Weyhenmeyer and B. T. Cunningham, *Lab Chip*, 2012, **12**, 574–581.
- 23 K. E. Shafer-Peltier, C. L. Haynes, M. R. Glucksberg and R. P. Van Duyne, *J. Am. Chem. Soc.*, 2003, **125**, 588–593.
- 24 D. A. Stuart, J. M. Yuen, N. S. O. Lyandres, C. R. Yonzon, M. R. Glucksberg, J. T. Walsh and R. P. Van Duyne, *Anal. Chem.*, 2006, **78**, 7211–7215.
- 25 K. Ma, J. M. Yuen, N. C. Shah, J. T. Walsh, M. R. Glucksberg and R. P. Van Duyne, *Anal. Chem.*, 2011, **83**, 9146–9152.
- 26 O. Lyandres, N. C. Shah, C. R. Yonzon, J. T. Walsh, M. R. Glucksberg and R. P. Van Duyne, *Anal. Chem.*, 2005, **77**, 6134–6139.
- 27 K. Kneipp, A. S. Haka, H. Kneipp, K. Badizadegan, N. Yoshizawa, C. Boone, K. E. Shafer-Peltier, J. T. Motz, R. R. Dasari and M. S. Feld, *Appl. Spectrosc.*, 2002, **56**, 150–154.
- 28 W. Xie, L. Wang, Y. Y. Zhang, L. Su, A. Shen, J. Q. Tan and J. M. Hu, *Bioconjugate Chem.*, 2009, **20**, 768–773.
- 29 A. Barhoumi, D. Zhang, F. Tam and N. J. Halas, *J. Am. Chem. Soc.*, 2008, **130**, 5523–5529.
- 30 E. Papadopoulou and S. E. J. Bell, *Angew. Chem., Int. Ed.*, 2011, **50**, 9058–9061.
- 31 R. A. Alvarez-Puebla, R. Contreras-Caceres, I. Pastoriza-Santos, J. Perez-Juste and L. M. Liz-Marzan, *Angew. Chem., Int. Ed.*, 2009, **48**, 138–143.
- 32 L. Guerrini, J. V. Garcia-Ramos, C. Domingo and S. Sanchez-Cortes, *Anal. Chem.*, 2009, **81**, 953–960.
- 33 R. A. Alvarez-Puebla and L. M. Liz-Marzan, *Angew. Chem., Int. Ed.*, 2012, **51**, 11214–11223.
- 34 B. Küstner, M. Gellner, M. Schütz, F. Schöppler, A. Marx, P. Ströbel, P. Adam, C. Schmuck and S. Schlücker, *Angew. Chem., Int. Ed.*, 2009, **48**, 1950–1953.
- 35 S. Mahajan, J. Richardson, T. Brown and P. N. Bartlett, *J. Am. Chem. Soc.*, 2008, **130**, 15589–15601.
- 36 Y. W. C. Cao, R. C. Jin and C. A. Mirkin, *Science*, 2002, **297**, 1536–1540.
- 37 T. Kang, S. M. Yoo, I. Yoon, S. Y. Lee and B. Kim, *Nano Lett.*, 2010, **10**, 1189–1193.
- 38 H. Zhang, M. H. Harpster, H. J. Park and P. A. Johnson, *Anal. Chem.*, 2011, **83**, 254–260.
- 39 D. van Lierop, K. Faulds and D. Graham, *Anal. Chem.*, 2011, **83**, 5817–5821.
- 40 A. Jemal, R. Siegel, J. Q. Xu and E. Ward, *Ca-Cancer J. Clin.*, 2010, **60**, 277–300.
- 41 M. Andrianifahanana, N. Moniaux, B. M. Schmied, J. Ringel, H. Friess, M. A. Hollingsworth, M. W. Buchler, J. P. Aubert and S. K. Batra, *Clin. Cancer Res.*, 2001, **7**, 4033–4040.
- 42 G. F. Wang, R. J. Lipert, M. Jain, S. Kaur, S. Chakraborty, M. P. Torres, S. K. Batra, R. E. Brand and M. D. Porter, *Anal. Chem.*, 2011, **83**, 2554–2561.
- 43 H. Hwang, H. Chon, J. Choo and J. K. Park, *Anal. Chem.*, 2010, **82**, 7603–7610.
- 44 M. C. Wu, *Nat. Photonics*, 2011, **5**, 322–324.
- 45 V. L. Schmit, R. Martoglio and K. T. Carron, *Anal. Chem.*, 2012, **84**, 4233–4236.
- 46 J. B. Song, J. J. Zhou and H. W. Duan, *J. Am. Chem. Soc.*, 2012, **134**, 13458–13469.
- 47 B. M. Discher, Y. Y. Won, D. S. Ege, J. C. M. Lee, F. S. Bates, D. E. Discher and D. A. Hammer, *Science*, 1999, **284**, 1143–1146.
- 48 C. Sheridan, H. Kishimoto, R. K. Fuchs, S. Mehrotra, P. Bhat-Nakshatri, C. H. Turner, R. Goulet, S. Badve and H. Nakshatri, *Breast Cancer Res.*, 2006, **8**, R59.
- 49 K. Lee, V. P. Drachev and J. Irudayaraj, *ACS Nano*, 2011, **5**, 2109–2117.
- 50 M. A. Woo, S. M. Lee, G. Kim, J. Baek, M. S. Noh, J. E. Kim, S. J. Park, A. Minai-Tehrani, S. C. Park, Y. T. Seo, Y. K. Kim, Y. S. Lee, D. H. Jeong and M. H. Cho, *Anal. Chem.*, 2009, **81**, 1008–1015.
- 51 W. T. Lu, A. K. Singh, S. A. Khan, D. Senapati, H. T. Yu and P. C. Ray, *J. Am. Chem. Soc.*, 2010, **132**, 18103–18114.
- 52 M. Y. Sha, H. X. Xu, M. J. Natan and R. Cromer, *J. Am. Chem. Soc.*, 2008, **130**, 17214–17215.

- 53 D. R. Shaffer, M. A. Leversha, D. C. Danila, O. Lin, R. Gonzalez-Espinoza, B. Gu, A. Anand, K. Smith, P. Maslak, G. V. Doyle, L. W. M. M. Terstappen, H. Lilja, G. Heller, M. Fleisher and H. I. Scher, *Clin. Cancer Res.*, 2007, **13**, 2023–2029.
- 54 S. Schlücker, B. Küstner, A. Punge, R. Bonfig, A. Marx and P. Ströbel, *J. Raman Spectrosc.*, 2006, **37**, 719–721.
- 55 M. Schütz, D. Steinigeweg, M. Salehi, K. Kömpe and S. Schlücker, *Chem. Commun.*, 2011, **47**, 4216–4218.
- 56 N. Stone, K. Faulds, D. Graham and P. Matousek, *Anal. Chem.*, 2010, **82**, 3969–3973.
- 57 N. Stone, M. Kerssens, G. R. Lloyd, K. Faulds, D. Graham and P. Matousek, *Chem. Sci.*, 2011, **2**, 776–780.
- 58 X. M. Qian, X. H. Peng, D. O. Ansari, Q. Yin-Goen, G. Z. Chen, D. M. Shin, L. Yang, A. N. Young, M. D. Wang and S. M. Nie, *Nat. Biotechnol.*, 2008, **26**, 83–90.
- 59 R. McQueenie, R. Stevenson, R. Benson, N. MacRitchie, I. McInnes, P. Maffia, K. Faulds, D. Graham, J. Brewer and P. Garside, *Anal. Chem.*, 2012, **84**, 5968–5975.
- 60 M. V. Yigit, L. Y. Zhu, M. A. Ifediba, Y. Zhang, K. Carr, A. Moore and Z. Medarova, *ACS Nano*, 2011, **5**, 1056–1066.
- 61 M. F. Kircher, A. de la Zerda, J. V. Jokerst, C. L. Zavaleta, P. J. Kempen, E. Mittra, K. Pitter, R. M. Huang, C. Campos, F. Habte, R. Sinclair, C. W. Brennan, I. K. Mellinghoff, E. C. Holland and S. S. Gambhir, *Nat. Med.*, 2012, **18**, 829–835.
- 62 A. Samanta, K. K. Maiti, K. S. Soh, X. J. Liao, M. Vendrell, U. S. Dinish, S. W. Yun, R. Bhuvaneswari, H. Kim, S. Rautela, J. H. Chung, M. Olivo and Y. T. Chang, *Angew. Chem., Int. Ed.*, 2011, **50**, 6089–6092.
- 63 J. Dong, Q. F. Chen, C. H. Rong, D. Y. Li and Y. Y. Rao, *Anal. Chem.*, 2011, **83**, 6191–6195.
- 64 S. E. J. Bell and M. R. McCourt, *Phys. Chem. Chem. Phys.*, 2009, **11**, 7455–7462.
- 65 W. Xie, B. Walkenfort and S. Schlücker, *J. Am. Chem. Soc.*, 2013, **135**, 1657–1660.
- 66 D. Steinigeweg, M. Schütz, M. Salehi and S. Schlücker, *Small*, 2011, **7**, 2443–2448.
- 67 S. J. Soenen, B. Manshian, J. M. Montenegro, F. Amin, B. Meermann, T. Thiron, M. Cornelissen, F. Vanhaecke, S. Doak, W. J. Parak, S. De Smedt and K. Braeckmans, *ACS Nano*, 2012, **6**, 5767–5783.
- 68 Y. Pan, S. Neuss, A. Leifert, M. Fischler, F. Wen, U. Simon, G. Schmid, W. Brandau and W. Jahnen-Dechent, *Small*, 2007, **3**, 1941–1949.
- 69 E. E. Connor, J. Mwamuka, A. Gole, C. J. Murphy and M. D. Wyatt, *Small*, 2005, **1**, 325–327.
- 70 X. X. Han, B. Zhao and Y. Ozaki, *Anal. Bioanal. Chem.*, 2009, **394**, 1719–1727.
- 71 E. Papadopoulou and S. E. J. Bell, *Chem.–Eur. J.*, 2012, **18**, 5394–5400.
- 72 X. X. Han, G. G. Huang, B. Zhao and Y. Ozaki, *Anal. Chem.*, 2009, **81**, 3329–3333.
- 73 J. D. Driskell, K. M. Kwarta, R. J. Lipert, M. D. Porter, J. D. Neill and J. F. Ridpath, *Anal. Chem.*, 2005, **77**, 6147–6154.
- 74 D. Graham and K. Faulds, *Expert Rev. Mol. Diagn.*, 2009, **9**, 537–539.
- 75 M. Li, J. M. Zhang, S. Suri, L. J. Sooter, D. L. Ma and N. Q. Wu, *Anal. Chem.*, 2012, **84**, 2837–2842.
- 76 G. Chen, Y. Wang, M. X. Yang, J. Xu, S. J. Goh, M. Pan and H. Y. Chen, *J. Am. Chem. Soc.*, 2010, **132**, 3644–3645.
- 77 M. Gellner, D. Steinigeweg, S. Ichilmann, M. Salehi, M. Schütz, K. Kömpe, M. Haase and S. Schlücker, *Small*, 2011, **7**, 3445–3451.
- 78 L. G. Xu, H. Kuang, C. L. Xu, W. Ma, L. B. Wang and N. A. Kotov, *J. Am. Chem. Soc.*, 2012, **134**, 1699–1709.